SCIENTIFIC REPORTS

OPEN

SUBJECT AREAS:
ATTRIBUTION
ENVIRONMENTAL SCIENCES

Received
13 May 2014

Accepted
23 September 2014

Published
6 November 2014

Correspondence and requests for materials should be addressed to S.Y. (shaocaiyu@zju.edu.cn)

Attribution of the United States "warming hole": Aerosol indirect effect and precipitable water vapor

Shaocai Yu[1], Kiran Alapaty[2], Rohit Mathur[2], Jonathan Pleim[2], Yuanhang Zhang[3], Chris Nolte[2], Brian Eder[2], Kristen Foley[2] & Tatsuya Nagashima[4]

[1]Research Center for Air Pollution and Health, College of Environmental and Resource Sciences, Zhejiang University, Hangzhou, Zhejiang 310058, P.R. China, [2]Atmospheric Modeling and Analysis Division, National Exposure Research Laboratory, U.S. Environmental Protection Agency, Research Triangle Park, NC 27711, USA, [3]College of Environmental Sciences and Engineering, Peking University, Beijing 100871, China, [4]National Institute for Environmental Studies, Tsukuba-shi, Ibaraki 305-8506, Japan.

Aerosols can influence the climate indirectly by acting as cloud condensation nuclei and/or ice nuclei, thereby modifying cloud optical properties. In contrast to the widespread global warming, the central and south central United States display a noteworthy overall cooling trend during the 20th century, with an especially striking cooling trend in summertime daily maximum temperature (T_{max}) (termed the U.S. "warming hole"). Here we used observations of temperature, shortwave cloud forcing (SWCF), longwave cloud forcing (LWCF), aerosol optical depth and precipitable water vapor as well as global coupled climate models to explore the attribution of the "warming hole". We find that the observed cooling trend in summer T_{max} can be attributed mainly to SWCF due to aerosols with offset from the greenhouse effect of precipitable water vapor. A global coupled climate model reveals that the observed "warming hole" can be produced only when the aerosol fields are simulated with a reasonable degree of accuracy as this is necessary for accurate simulation of SWCF over the region. These results provide compelling evidence of the role of the aerosol indirect effect in cooling regional climate on the Earth. Our results reaffirm that LWCF can warm both winter T_{max} and T_{min}.

A major barrier to reliable prediction of climate change on decadal and longer scales is the characterization of uncertainties in the magnitude of the estimated cloud-mediated (indirect) effects of aerosols[1]. The aerosol indirect effect can be negative or positive by suppressing or invigorating the development of clouds and precipitation under different circumstances due to the complex interaction between aerosols and cloud droplets[2,3]. Airborne absorbing aerosols have been reported to raise regional temperature by reducing the local large-scale cloud cover[1]. The competing radiative effects of climate include the greenhouse effect (warming due to infrared absorbers) and the "whitehouse" effect (cooling due to visible wavelength reflectors)[1]. As reflectors, clouds affect the climate by reflecting incoming solar radiation back to space (shortwave cloud forcing (SWCF)), which tends to decrease the daytime maximum surface temperature (T_{max}) (cooling effect), and by trapping outgoing infrared radiation (longwave cloud forcing (LWCF)), which tends to increase both nighttime minimum (T_{min}) and daytime T_{max} (warming effect). In addition, the increase of infrared absorbers such as greenhouse gases (e.g., CO_2 and precipitable water vapor (Q)) and absorbing aerosol results in an increase in both daytime T_{max} and nighttime T_{min} (warming effect due to longwave forcing), whereas the increase of visible reflectors such as sulfate aerosols and clouds leads to a decrease of the daytime T_{max} (cooling effect due to shortwave forcing)[4–6]. If the infrared absorption dominates and consequently the greenhouse effect increases, both nighttime T_{min} and daytime T_{max} should increase with potentially larger effects during the winter due to its longer nights and more stable lapse rate[7]. If the visible reflection dominates and the whitehouse effect increases, the daytime T_{max} should decrease, primarily when solar radiation is the greatest (summer)[6,7].

In contrast to the widespread global warming, the central and south central United States display a noteworthy overall cooling trend over the past century, with an especially striking cooling trend in summertime daily T_{max} (termed the U.S. "warming hole")[1,8,9] (also Supplementary Fig. S1A and Supplementary Note 1). Several explanations have been suggested for this cooling trend, which seem partly associated with the change in sea surface temperatures[10], low-level circulations/soil moisture feedback[9], internal dynamic variability[11], the change in cumulus clouds[12], the positive low-level moisture convergence[13], large-scale circulation modes (El Nino/

Southern Oscillation)[8] and land surface processes[14]. It has been speculated that the aerosol direct and indirect effects play a significant role in the observed strong anticorrelation between trends in summer daily T_{max} and precipitation in these regions[8]. The strong anticorrelation between precipitation and Tmax (and diurnal temperature range) during the warm season has also been found in many other regions[15,16].

Results

Here we use monthly mean observational data sets of T_{max} and T_{min} from the Global Historical Climatology Network Monthly (GHCNM)[17], cloud properties (SWCF and LWCF at the top of atmosphere (TOA), cloud optical depth (COD) and cloud fractions) from the Clouds and Earth's Radiant Energy System (CERES)[18], aerosol optical depth (AOD) from Terra-MODIS, Q from, National Center for Environmental Prediction (NCEP) reanalysis data, and global coupled climate models (Supplementary Notes 1, 2, 3) to explore the attribution of the U.S. "warming hole". The very strong correlation between summer T_{max} and SWCF (correlation coefficient (r) $>$ 0.67 is statistically significant at the 0.05 level) in the scatter plots of Fig. 1A during 2000–2011 is a strong indication that SWCF is one of the major driving forces for the noted variability in summer T_{max} over the continental U.S. (CONUS). This is strongly supported by a nearly perfect match of negative trends in the western U.S (WUS) and positive trends in the eastern U.S. (EUS) for summer T_{max} and SWCF with the U.S. High Plains dryline as separation. The negative trends in summer T_{max} in Maine are collocated with consistent negative trends in SWCF (Figs. 2A and 2B). This is confirmed by the consistent longitudinal variation of the trends of summer T_{max}, and SWCF in Fig. 1C. This is evidence that the SWCF trends are one of the main causes for negative trends in WUS and positive trends in EUS for summer T_{max}. Fig. 1A strongly supports the assumption that response of temperature to the climate forcing is proportional[7,19]. Since SWCF by definition is negative, the positive slope (0.12 ± 0.002 (2σ) and 0.15 ± 0.003°C/(W/m^2) for EUS and WUS, respectively) means that during summer, when solar radiation is the greatest, more clouds can reflect more incoming solar radiation back to space (larger negative SWCF values), systematically decreasing the daytime T_{max} significantly over the CONUS.

One obvious question remains as to what causes the observed regional scale change in clouds. Although all cloud droplets must form on preexisting aerosol particles that act as cloud condensation nuclei (CCN)[3], cloud distributions depend not only on the available aerosol particles that serve as CCN but also on prevalent atmospheric dynamic and thermodynamic processes[3,20]. Although there is substantial evidence of the aerosol indirect effect (AIE)[2,3,21–26], the summer T_{max} can change because of variation in large-scale atmospheric circulation. Following Kaufman et al.[27], a multiple linear regression (MLR) is used to analyze the influence of synoptic meteorological parameters (from NCEP reanalysis) and aerosols on summer T_{max}, its trends and SWCF trends as listed in Table 1 (Supplementary Note 11). Note that the correlations between variables do not prove causality and that the aerosol indirect effect on climate cannot be untangled with high degree of confidence until regional climate models can predict climate change and cloud evolution with high precision. Table 1 indicates SWCF and Q are the two major contributors to variability in both summer T_{max} (β-coefficients for relative importance are 0.48 and 0.44, respectively) and its trends (β-coefficients are 0.38 and 0.37, respectively) over the CONUS. This is supported by very significant linear correlations between summer T_{max} and Q over the EUS in Fig. 3 and the nearly perfect match of positive trends in EUS for summer T_{max} and Q in Figs. 2A and 2E except the northeast portion of U.S. Q is considered as the most important greenhouse gas with positive feedback[1] (Supplementary Note 10). The results within and outside the "warming hole" are similar to those over the CONUS except that Q is not important for summer T_{max} for outside the "warming hole" as shown in Table 1 and Fig. S14B. The results in Table 1 further reveal that the aerosol direct effect calculated by a box model[28] (Supplementary Note 6) does not play a significant role in decreasing summer T_{max} over the CONUS, in agreement with other studies[7,13,29]. The very poor correlations between moisture convergence and summer T_{max} (Supplementary Figs. S11 and S12, Supplementary Note 9) indicate unimportance of the moisture convergence for the summer T_{max} and U.S. "warming hole".

A high population density and energy, and combustion-related atmospheric emissions interspersed with heavily forested areas in the EUS provide precursors and sources of anthropogenic and biogenic inorganic and organic aerosols[30–33], which can be CCN. The close match of negative trends in summer AOD and positive trends in SWCF over the source regions of the central and eastern U.S. in Figs. 2B and 2D is strong evidence that the AOD trends are the main cause of positive trends in SWCF during 2000–2011. This is confirmed by the consistent longitudinal variation of the negative trends in both AOD and COD, and positive trends in SWCF over the EUS in Fig. 1C and significant linear correlations between the trends of longitudinal mean AOD and mean SWCF in Fig. 1D (Supplementary Fig. S6). Table 1 shows that the trends of AOD are mainly responsible for the variability in the trend of SWCF and the variability of longitudinal means of SWCF trends.

To explain the attribution of the "warming hole" for the period of 1950 to 2011 (Supplementary Fig. S1A) (or 1901 to 2011 (Supplementary Fig. S5A)), we analyze available results of nineteen global coupled models from the World Climate Research Programme's (WCRP's) Coupled Model Intercomparison Project phase 5 (CMIP5) multimodel data set[34] for both periods of 2000 to 2011 and 1950 to 2011 (Supplementary Notes 12, 2). Fig. 1B shows the scatter plots from the simulations of the MIROC-ESM-CHEM model for the period of 1950 to 2011. Similar to the observations, very strong linear correlations are noted for summer T_{max}-SWCF in all models as listed in Supplementary Table S1 except the CESM1-CAM5-1-FV, which exhibits a comparatively smaller slope and weak correlation. The observed slopes for 2000 to 2011 fall within the range estimated from the models with substantial agreement between the observations and models. The model results show apparent independence of the period of analysis in the slopes and correlations as evidenced by similar slopes and correlations for both periods. Thus, we can confidently conclude that the observed slopes and correlations for summer T_{max}-SWCF for 2000 to 2011 in Fig. 1 are representative of those for the longer timescale (1950 to 2011).

Nationally, SO_2 emissions grew from 1950 to about 1980 and then decreased by more than 60% between 1980 and 2010[30] and there is a linear relationship between decreasing aerosol sulfate concentrations and SO_2 emissions[30]. This is in agreement with the observations that for summer T_{max} in EUS, there are almost uniformly negative trends during 1950–1985 (Fig. 4E) in contrast to almost uniformly positive trends during 1985–2011 (Supplementary Fig. S41I) and 2000 to 2011 (Fig. 2A). This is supported by the fact that over the United States cloud cover has increased from 1949 to 2001 in summer and annual means with all of this increase occurring prior to the early 1980s[35]. The trend analyses for the global coupled models from CMIP5 (Supplementary Note 12) indicate that only MIROC-ESM-CHEM model successfully shows negative trends in summer T_{max} (i.e., the U.S. "warming hole") (Figs. 4A for the observations, and S39A for the models) and SWCF (Fig. 4B) over the central U.S. during 1950–2011. Detailed analysis (Supplementary Note 13) shows that our MIROC-ESM-CHEM model successfully and consistently reproduced the observed summer features for the long-term (i.e., "warming hole" over the central U.S. for the 1901–2011 (Supplementary Fig. S38) and 1950–2011 periods (Supplementary Fig. S39) and negative trends in T_{max} over the EUS for the 1950–1985 period with positive trends in AOD and negative trends in SWCF

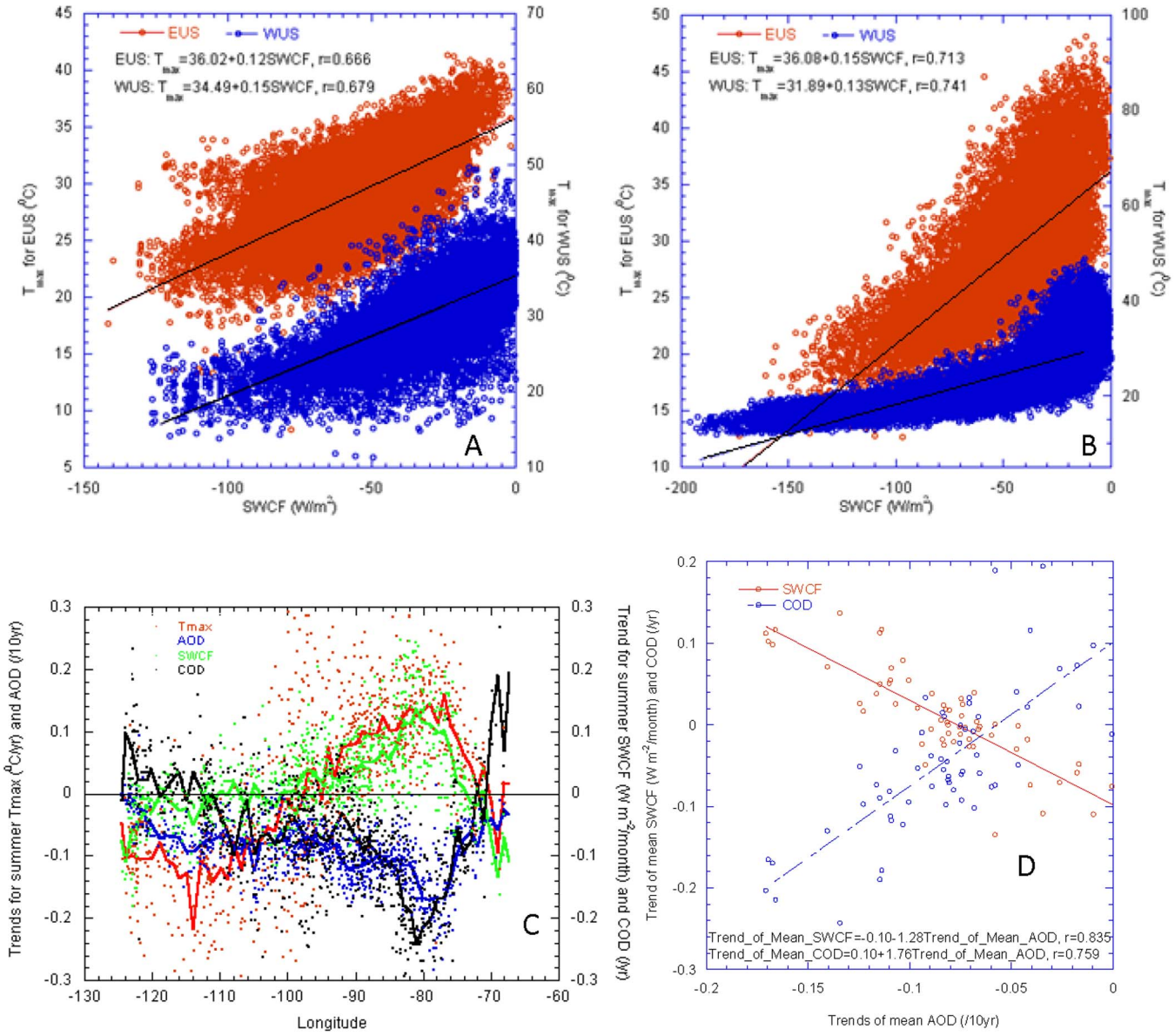

Figure 1 | (A) Scatter plots of monthly mean T_{max} versus SWCF on the basis of the observations from CERES and GHCNM for the summer (June–August) between March 2000 and December 2011. (B) Scatter plot of monthly mean T_{max} versus SWCF from the MIROC-ESM-CHEM model simulation for the summer between January 1950 and December 2011. (C) longitude variation of trends for monthly mean T_{max}, SWCF, COD and AOD on the basis of the observations from CERES, GHCNM and MODIS for the summer (June–August) between March 2000 and December 2011. Solid lines show the averaged results and the points show the individual stations. (D) Correlation between trends of AOD and SWCF and COD for averaged results of the solid lines in (C). In this study, EUS and WUS refer to the eastern United States (longitude: 100°W to 60°W; latitude: 25°N to 50°N) and the west U.S. (longitude: 130°W to 100°W; latitude for summer: 25°N to 50°N and latitude for winter: 36°N to 50°N), respectively.

(Supplementary Fig. S40) and for the short-term of 2000–2011 for T_{max} (positive trends), AOD (negative trends), SWCF (positive trends) and Q (positive trends in southeast and negative trends in northeast) over the EUS (Supplementary Fig. S43, Supplementary Note 13). MIROC-ESM-CHEM missed the "warming hole" over the south central U.S. during the 1950–2011 period because MIROC-ESM-CHEM did not include the AIE on subgrid convective clouds and this effect is dominantly important over the south central U.S.[36–38]. On contrary, MIROC-ESM did not capture the "warming hole" for the 1950–2011 (Supplementary Fig. S39) and other observed features such as Q for the 2000–2011 period (Supplementary Fig. S43) because of different distributions of AOD and SWCF from the MIROC-ESM simulations (Supplementary Figs. S39G and S39F) relative to those from the MIROC-ESM-CHEM (Supplementary Figs. S39C and S39B). Comparisons of distribution patterns from the MIROC-ESM-CHEM and MIROC-ESM simulations (Supplementary Note 13), especially for AOD and SWCF, indicate that the results of AOD and SWCF from the MIROC-ESM simulations are not in right locations as shown in Supplementary Figs. S39G and S39F relative to those from the MIROC-ESM-CHEM (see Supplementary Figs. S39C and S39B) for the 1950–2011 period. The results from the MIROC-ESM-CHEM showed the positive trends in AOD over the central U.S. while MIROC-ESM-CHEM showed the negative trends in AOD over the central U.S. for the 1950–2011 period. This difference causes the different results for the SWCF and T_{max} as shown in Supplementary Fig. S39. Since the only difference between MIROC-ESM-CHEM and MIROC-ESM is that the MIROC-ESM

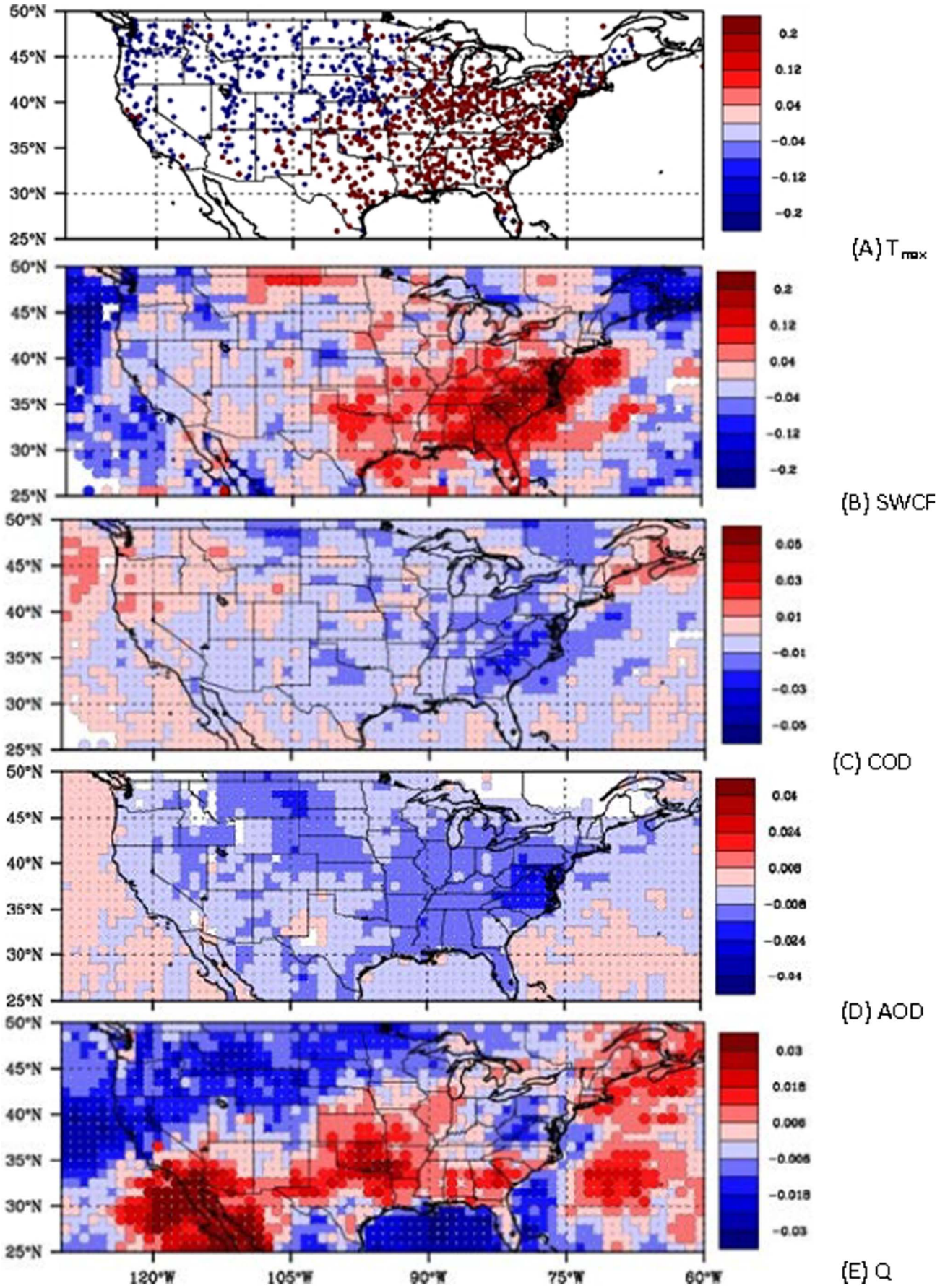

Figure 2 | The trends in summer monthly mean (A) T_{max}, (see enlarged plot in Supplementary Information) (B) SWCF, (C) COD, (D) AOD and (E) Q for the period 2000–2011 on the basis of GHCNM (T_{max}), CERES (SWCF, COD) and Terra-MODIS (AOD, Q) data sets. The units for trends of T_{max}, SWCF, COD, AOD and Q are °C/100 yrs, (W/m^2)/month, /month, /yr, and cm/year, respectively. The maps were created by NCAR Command Language (NCL) (http://www.ncl.ucar.edu/).

Table 1 | MLR analysis of the influence of meteorological parameters on monthly mean T_{max}, and trends of monthly mean T_{max} (the results in parentheses) and SWCF over the CONUS, "warming hole" (−100°W to −75°W) and outside (<−100°W or >−75°W) (SOM)

	Over CONUS		Warming hole		Outside	
T_{max}						
	CC to T_{max}	β by MLR	CC to T_{max}	β by MLR	CC to T_{max}	β by MLR
SWCF	0.60(0.68)	0.48 ± 0.00(0.38 ± 0.02)	0.64(0.61)	0.27 ± 0.00(0.29 ± 0.04)	0.69(0.37)	0.53 ± 0.01(0.39 ± 0.04)
Uwnd500	−0.53(0.22)	−0.10 ± 0.01	−0.69(−0.27)	−0.35 ± 0.01	−0.38(0.15)	−0.43 ± 0.02
Uwnd700	−0.48(0.21)	−0.01 ± 0.01	−0.64(−0.17)	0.30 ± 0.01	−0.38(−0.16)	0.31 ± 0.02
ADF	−0.46(0.02)	−0.13 ± 0.00	−0.38(−0.01)	−0.06 ± 0.00	−0.52(−0.36)	−0.21 ± 0.01(−0.37 ± 0.04)
Q	0.41(0.52)	0.44 ± 0.00(0.37 ± 0.02)	0.72(0.31)	0.52 ± 0.00(0.23 ± 0.03)	0.16(0.56)	
Vwnd1000	0.36(−0.18)	0.07 ± 0.00	0.51(0.30)	0.07 ± 0.00(0.27 ± 0.03)	0.23(0.51)	
Uwnd1000	−0.34(−0.11)	−0.04 ± 0.00	−0.44(−0.43)	−0.13 ± 0.00(−0.23 ± 0.03)	−0.22(−0.24)	
Pottmp500_925	−0.30(−0.59)	−0.22 ± 0.01(−0.34 ± 0.02)	−0.30(−0.63)	−0.15 ± 0.01(−0.25 ± 0.04)	−0.44(−0.26)	−0.15 ± 0.01(−0.16 ± 0.04)
Stat1000_700	0.30(0.28)	−0.00 ± 0.00	0.49(0.36)	0.09 ± 0.00(0.09 ± 0.04)	0.27(0.05)	
Vwnd700	0.23(−0.10)		0.32(−0.10)	−0.02 ± 0.00	0.29(0.12)	
Vwnd500	0.04(−0.12)		0.11(−0.42)		0.13(0.22)	
CC for MLR		0.83 (0.81)		0.90(0.79)		0.77(0.57)
Number	41501(924)	41501(924)	24648(569)	24648(569)	16853(355)	16853(355)
SWCF trend						
	CC to SWCF trend	β by MLR	β by MLR for longitude mean			
Trend of AOD	−0.45	−0.36 ± 0.03	−0.71 ± 0.12			
Trend of Stat1000_700	0.36	0.20 ± 0.03	0.07 ± 0.13			
Trend of vwnd700	−0.31	−0.002 ± 0.05	−0.16 ± 0.20			
Trend of vwnd500	−0.27	−0.11 ± 0.05	0.06 ± 0.18			
Trend of uwnd700	0.18					
Trend of vwnd1000	−0.14					
Trend of uwnd500	0.11					
Trend of uwnd1000	0.01					
CC for MLR		0.51	0.83			
Number	924	924	58			

Uwnd1000, uwnd700, uwnd500, vwnd1000, vwnd700, vwnd500, Q, Pottmp500_925, Stat100_700, and ADF represent easternly wind at 1000 hpa, 700 hpa, 500 hpa, northernly wind at 1000 hpa, 700 hpa, 500 hpa, precipitable water vapor, potential temperature difference at 500–950 hpa, low static stability at 1000–700 hpa, and aerosol direct forcing, respectively. "CC" means correlation coefficient. "β" (estimate ± standard error) means standardized β-coefficients in MLR which show the relative contribution of the predictors on a scale ranging from −1 to 1 (SOM). "0.00" means "<0.005".

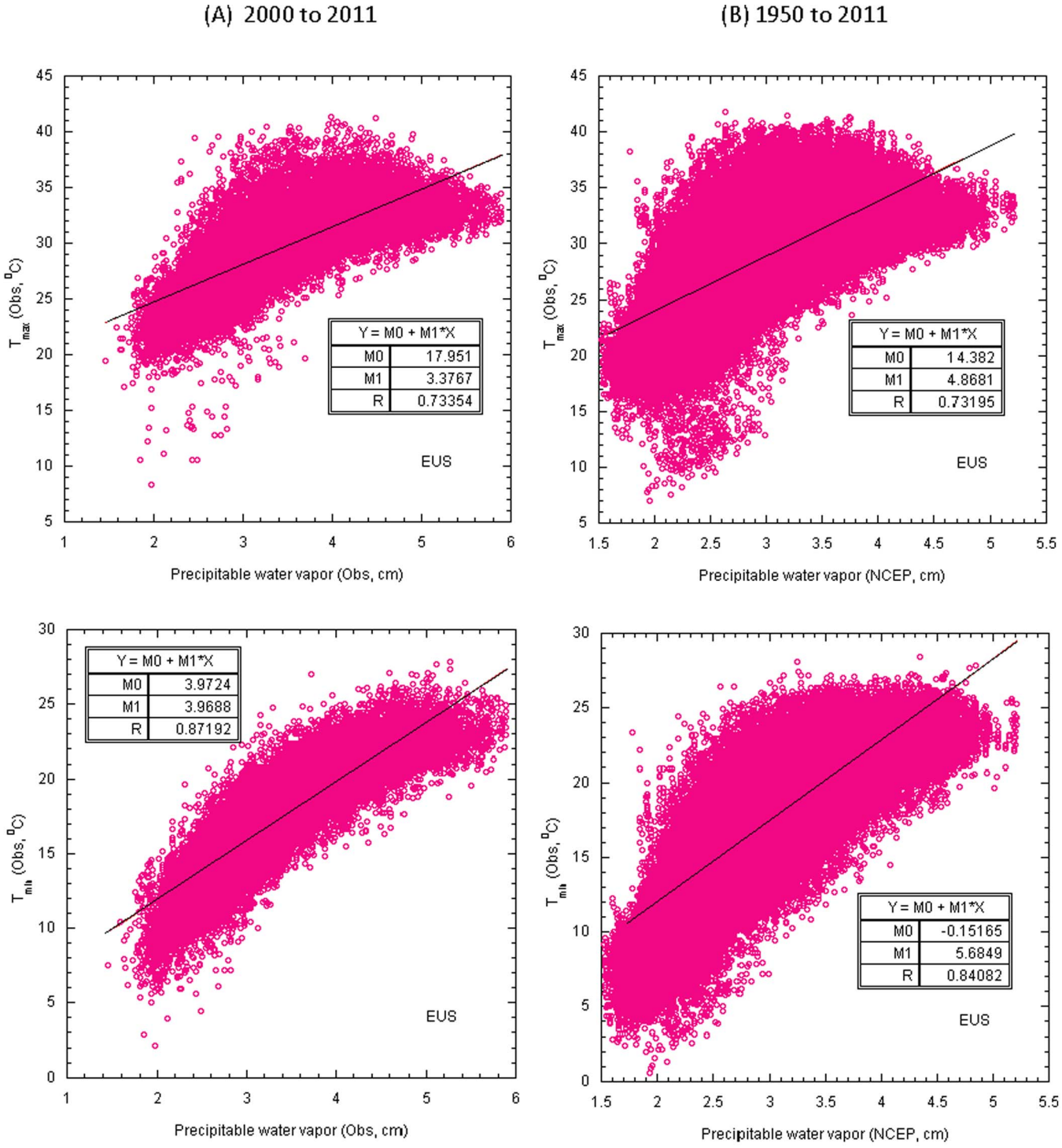

Figure 3 | Scatter plots of summer monthly mean precipitable water vapor (Q) versus observed T_{max} and T_{min} at the GHCNM sites over the EUS for (A) 2000 to 2011 (Q data are based on the observations from the Terra-MODIS) and (B) 1950 to 2011 (Q data are based on NCEP/NCAR reanalysis). All temperature data are based on the observations from the GHCNM.

simulations used prescribed monthly mean 3-D chemical fields while the MIROC-ESM-CHEM simulations used chemical fields calculated by the online photochemical module (Supplementary Note 13). Since good chemical fields will affect greenhouse gases such as H_2O and aerosol (AOD) fields, the much better performance of MIROC-ESM-CHEM relative to MIROC-ESM suggests the attribution of the "warming hole" to aerosol indirect effect (Supplementary Note 13). The U.S. "warming hole" (i.e. the decrease of summer T_{max}) over the central and south central U.S. regions in Fig. 4A is caused by the increase of clouds (Fig. 4B) due to increase of aerosols (Fig. 4C) with offset from the greenhouse effect of Q (increase of Q) (Fig. 4D) during 1950 to 2011 (Supplementary Notes 11, 13). The consistent cooling trends in summer T_{max} in EUS during 1950–1985 (Fig. 4E) are because of both increase of clouds (Fig. 4F) due to increase of aerosols (Fig. 4G) and decrease of Q (Fig. 4H) (Supplementary Notes 11, 13).

In addition, the very strong linear correlation between winter T_{min} (T_{max}) and LWCF ($r > 0.65$ is statistically significant at the 0.05 level)

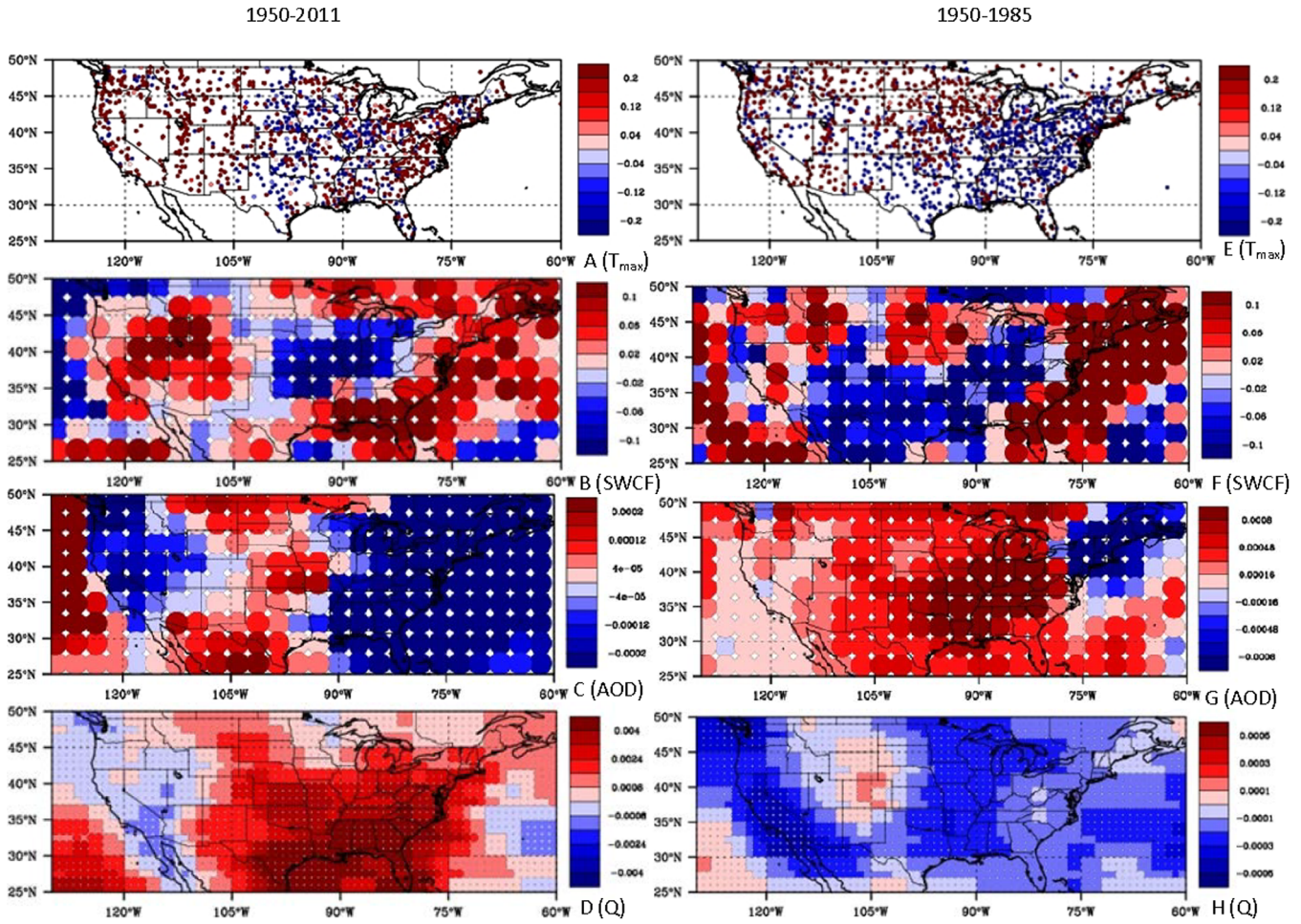

Figure 4 | The trends in summer monthly mean T_{max}, SWCF, AOD and Q for the period 1950–2011 (A, B, C, D, right column) and 1950–1985 (E, F, G, H, left column) on the basis of GHCNM (T_{max}), MIROC-ESM-CHEM (AOD at 550 nm, SWCF) and NCEP/NCAR reanalysis (Q) data sets. The units for trends of T_{max}, SWCF, AOD and Q are °C/100 yrs, (W/m^2)/yr, /yr and cm/yr, respectively. The maps were created by NCAR Command Language (NCL) (http://www.ncl.ucar.edu/).

in Figs. 5A and 5B for the 2000–2011 period shows that LWCF is one of the major driving forces for the noted change in winter T_{min} (T_{max}) in the region restricted to latitudes $\geq 36°$N because of latitudinal dependence of the climate response to radiative forcing[7,19,20]. A global study shows that a radiative forcing can yield a larger response at high latitude than at low latitude because of sea ice feedback and more stable lapse rate at high latitude, especially with calculated clouds[7]. Since LWCF by definition is positive, the positive slopes here imply that during the winter, more clouds can trap more outgoing infrared radiation, systematically increasing both nighttime T_{min} and daytime T_{max} significantly over the CONUS at latitudes $\geq 36°$N. This is supported by a nearly perfect match of consistent negative and positive trends in T_{min} and T_{max} with those of LWCF over the CONUS at latitudes $> 36°$N (Supplementary Fig. S9), indicating that the climate changes in these regions are more complicated and should be analyzed separately. The model results in Figs. 5C and 5D and Supplementary Table S1 show that the observed slopes and correlations for winter T_{min}-LWCF and winter T_{max}-LWCF for 2000 to 2011 are representative of those for the longer timescale (1950 to 2011). The summer AODs decrease over the CONUS, especially in the EUS (Fig. 5D), whereas the winter AODs increase at latitude $>$ 36°N (Supplementary Fig. S9) from 2000 to 2011. Over the ocean outside of the CONUS both summer and winter AOD increase (Fig. 2D for summer and Supplementary Fig. S9 for winter). The results over the WUS are similar to those of the EUS but with slightly smaller slopes and lower correlation coefficients, indicating that the response of winter T_{max} and T_{min} to LWCF is slightly weaker in the WUS than the EUS.

Discussion

We have strived to explore the attribution of the U.S. "warming hole" by using observations of temperature, SWCF, LWCF, AOD and precipitable water vapor as well as nineteen global coupled climate models. Our analysis shows that there are a very strong correlation between summer T_{max} and SWCF and a nearly perfect match of negative trends in the WUS and positive trends in the EUS for them during 2000–2011 over the CONUS. Note that the correlation (0.64) between SWCF and summer T_{max} is higher than that (0.46) between cloud fraction and summer T_{max} over the eastern U.S. as shown in Supplementary Fig. S44, indicating that SWCF is better variable in terms of change of summer T_{max}. On the other hand, Quuass et al. (2009)[39] pointed out that the positive strong correlation between AOD and cloud fraction may be due to the aerosol cloud lifetime effect, dynamical influences such as convergence, humidity welling and the bias in the satellite retrievals and none of these can provide a unique explanation. The MLR analysis shows that SWCF and precipitable water vapor are the two major contributors to variability in both summer T_{max} and its trends over the CONUS. It is found that there are the consistent longitude variation of the negative trends in both AOD and COD and significant linear correlation between the trends of longitudinal mean AOD and SWCF. This indicates that the trends of AOD are mainly responsible for the variability in the trends

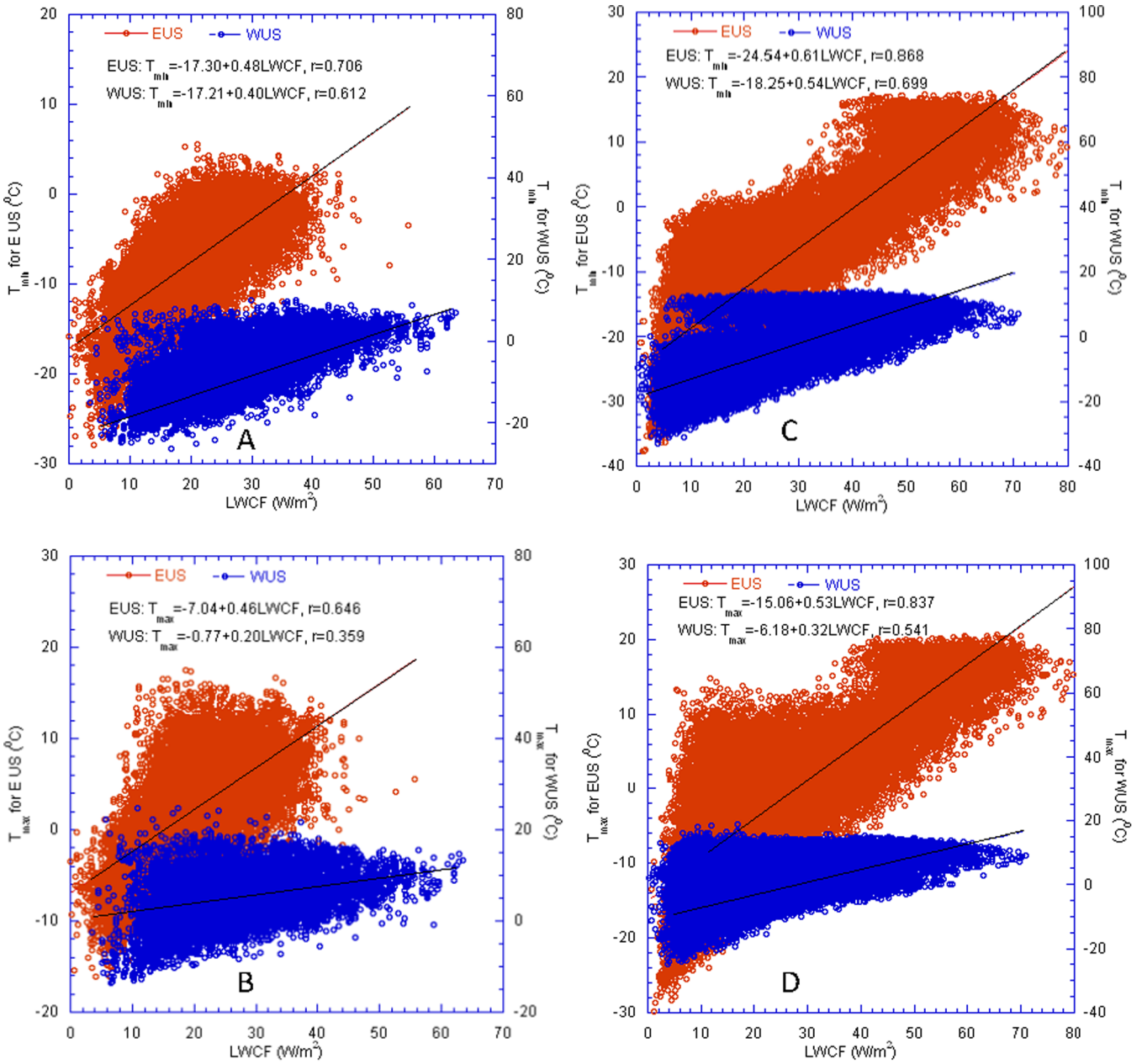

Figure 5 | Scatter plots of monthly mean LWCF versus (A) T_{min} and (B) T_{max} on the basis of the observations from CERES and GHCNM for the winter (December–February) from 2000 to 2011. Scatter plots of monthly mean LWCF versus (C) T_{min} and (D) T_{max} from the MOHC-HadGEM2-CC model simulation for the winter (December–February) from 1950 to 2011.

of SWCF and the variability of longitudinal means of SWCF trends. The MIROC-ESM-CHEM[36–38] coupled climate model (Supplementary Note 13) reveals that the observed "warming hole" (i.e., negative trend in summertime T_{max}) can be produced only when the aerosol fields are simulated reasonably as this is necessary for reasonable simulation of SWCF over the region. Since the purpose of this paper to analyze all CMIP5 GCMs models and show the results, more work is needed to prove the superiority of MIROC-ESM-CHEM. In conclusion, these results provide compelling evidence of the role of the aerosol indirect effect in cooling regional climate on the Earth.

On the other hand, many theoretical explanations about the attribution of the warming hole have been suggested. On the basis of analysis of 192 simulations from 22 CMIP5 climate models, Kumar et al.[40] found that models with relatively higher skill in simulating the North Atlantic low-frequency (multidecadal) oscillations are more likely to reproduce the warming hole over the North America. Leibensperger et al.[21] showed that the regional radiative forcing from the anthropogenic aerosols can cool the central and eastern U.S. by 0.5–1.0°C on average during 1970–1990 and that aerosol cooling can increase the southerly flow of moisture from the Gulf of Mexico which result in increased cloud cover and precipitation in the central U.S. This leads to largest cooling effect from the anthropogenic aerosols in the central U.S. The model simulations of Mickley et al.[41] over the U.S. for 2010–2050 found that removal of U.S. aerosols can cause significant regional warming with temperature during summer heat wave increasing by as much as 1–2 K in the northeastern U.S., in part, because of positive feedbacks involving soil moisture and low cloud cover. Pan et al.[9,14] believed that local/regional land-surface processes were partly responsible for the warming hole through their role in replenishment of seasonally depleted hydrologic cycle (soil moisture). Kunkel et al.[11] pointed out that the warming hole is assoc-

iated with variations in sea surface temperature (SSTs) in the tropic Pacific and that there was a strong association between the central U.S. temperatures and observed variability of North Atlantic SSTs. Lower SSTs over the North Atlantic can increase the anticyclonic transport of moisture from the Gulf of Mexico. Meehl et al.[13] believed that altered moisture convergence can increase precipitation with concomitant increases of soil moisture, surface evaporation and increased cloudiness. It is clear that all related works pointed to the fact that invoke changes in the moisture-aerosol-cloud-precipitation-SWCF interaction in the warming hole region. As stated in Rosenfeld et al[3], all cloud droplets must form on preexisting aerosol particles that act as CCN. This means that moisture needs aerosol particles to form clouds. To completely understand the moisture-aerosol-cloud-precipitation-SWCF interaction in the warming hole region, this will need more comprehensive models and is beyond of the scope of this work. Since the moisture-aerosol-cloud-precipitation-SWCF interaction is complicated, this interaction may be not linear. On the other hand, the southeast is upwind of the industrialized areas of the NE corridor, but is rich in aerosols from biogenic sources. Thus the possible greater moisture availability and the presence of sufficient aerosols (from both biogenic and anthropogenic sources) could provide for an ideal combination.

Methods

Observational datasets. We use the observational data of monthly mean maximum (T_{max}) and minimum (T_{min}) temperatures at thousands of stations (Supplementary Fig. S1) obtained from the Global Historical Climatology Network Monthly (GHCNM) version 3 (last updated: 04/11/2012) (http://www.ncdc.noaa.gov/ghcnm)[17]. The global monthly $1.0^\circ \times 1.0^\circ$ data for shortwave flux (all-sky, clear sky), longwave flux (all-sky, clear sky), cloud optical depth (COD), and cloud fractions under daytime and nighttime conditions at the TOA between March 2000 and December 2011 measured by the Clouds and the Earth's Radiant Energy System (CERES)[18] were downloaded from the NASA CERES website (http://ceres.larc.nasa.gov). The global monthly $1.0^\circ \times 1.0^\circ$ data for aerosol optical depth (AOD) at 550 nm and total precipitable water vapor between March 2000 and December 2011 on the basis of Terra-MODIS measurements were downloaded from the NASA Giovanni website (http://gdata1.sci.gsfc.nasa.gov/daac-bin/G3/gui.cgi?instance_id=aerosol_monthly). The global monthly $2.5^\circ \times 2.5^\circ$ mean meteorological fields for the period of 1950 to 2011 were downloaded from the National Center for Environmental Prediction (NCEP)/NCAR reanalysis website (http://www.esrl.noaa.gov/psd/data/reanalysis/reanalysis.shtml) (Supplementary Notes 1, 3).

Nineteen global coupled climate models. The global model results from the World Climate Research Programme's (WCRP's) Coupled Model Intercomparison Project phase 5 (CMIP5) multimodel data set[34] were obtained from the website (http://www-pcmdi.llnl.gov/ipcc/about_ipcc.php). Nineteen global climate models used in this work include GFDL-CM3, GFDL-ESM2G, NCAR-CCSM4, CESM1-CAM5-1-FV, NASA-GISS-E2-R, IPSL-CM5A-LR, INM-CM4, MPI-ESM-LR, MOHC-HadCM3, MOHC-HadGEM2-CC, MOHC-HadGEM2-ES, MRI-CGCM3, BCC-CSM1-1, NCC-NorESM1-M, CNRM-CM5, NIMR-KMA-HadGEM2, CSIRO-BOM-ACCESS1-0, MIROC-ESM-CHEM, and MIROC-ESM (Supplementary Note 2). Note that the analysis of the results of the CMIP5 GCMs uses a single member of the simulation ensemble from each GCM in this study. The model results from the historical (simulation of recent past)[34] and RCP45 (future projection forced by RCP (representative concentration pathway) 4.5 (radiative forcing of 4.5 W m^{-2})) runs were used for 1850 to 2005 and 2006 to 2011, respectively. The historical simulations (1850–2005) imposed changing conditions (consistent with observations) which may include[1] atmospheric composition (including CO_2) due to both anthropogenic and volcanic influences, solar forcing, emissions or concentrations of short-lived species and natural and anthropogenic aerosols or their precursors and land use[6,34]. On the other hand, the RCP45 future climate projections (2006–2100) identify a concentration pathway that approximately results in a radiative forcing of 4.5 W m^{-2} at year 2100, relative to pre-industrial conditions[6].

1. Solomon, S. *et al.* eds, *Climate Change 2007: The Physical Science Basis. Contribution of Working Group I to the Fourth Assessment Report of the Intergovernmental Panel on Climate Change* (Cambridge Univ Press, New York) (2007).
2. Stevens, B. & Feingold, G. Untangling aerosol effects on clouds and precipitation in a buffered system. *Nature* **461**, 607–613 (2009).
3. Rosenfeld, D. *et al.* Flood or drought: how do aerosols affect precipitation? *Science* **321**, 1309–1313 (2008).
4. Karl, T. R. *et al.* A new perspective on recent global warming: Asymmetric trends of daily maximum and minimum temperatures. *Bull. Amer. Met. Soc.* **74**, 1007–1023 (1993).
5. Easterling, D. R. *et al.* Climate extremes: Observations, modeling, and impacts. *Science* **289**, 2068–2074 (2000).
6. Yu, S. C., Saxena, V. K. & Zhao, Z. A comparison of signals of regional aerosol-induced forcing in eastern China and the southeastern United States. *Geophys. Res. Lett.* **28**, 713–716 (2001).
7. Hansen, J., Lacis, A. & Ruedy, R. Radiative Forcing and Climate Response. *J. Geophys Res.* **102**, 6831–6864 (1997).
8. Portmann, R. W., Solomon, S. & Hegerl, G. C. Spatial and seasonal patterns in climate change, temperatures, and precipitation across the United States. *Proc. Natl. Acad. Sci. USA* **106**, 7324–7329 (2009).
9. Pan, Z. *et al.* Altered hydrologic feedback in a warming climate introduces a "warming hole." *Geophys Res Lett* **31**, L17109, DOI:10.1029/2004GL020528 (2004).
10. Robinson, W. A., Reudy, R. & Hansen, J. E. General circulation model simulations of recent cooling in the east-central United States. *J Geophys Res* **107**, 4748, DOI:10.1029/2001JD001577 (2002).
11. Kunkel, K. E., Liang, X. Z., Zhu, J. & Lin, Y. Can CGCMs simulate the twentieth-century "warming hole" in the central United States. *J Climate* **19**, 4137–4153 (2006).
12. Liang, X. Z. *et al.* Regional climate model downscaling of the U.S. summer climate and future change. *J Geophys Res* **111**, D10108, DOI:10.1029/2005JD006685 (2006).
13. Meehl, G. A., Arblaster, J. M. & Branstator, G. Mechanisms Contributing to the Warming Hole and the Consequent U.S. East–West Differential of Heat Extremes. *J Climate* **25**, 6394–6408 (2012).
14. Pan, Z. *et al.* Intermodel variability and mechanism attribution of central and southeastern U.S. anomalous cooling in the twentieth century as simulated by CMIP5 models. *J. Climate* **26**, 6215–6237 (2013).
15. Trenberth, K. E. & Shea, D. J. Relationships between precipitation and surface temperature. *Geophys Res Lett* **32**, L14703, DOI:10.1029/2005GL019760 (2005).
16. Zhou, L., Dickinson, R. E., Tian, Y., Vose, R. & Dai, Y. Impact of vegetation removal and soil aridation on diurnal temperature range in a semiarid region—application to the Sahel. *Proc Natl Acad Sci USA* **104**, 17937–17942 (2007).
17. Lawrimore, J. H. *et al.* An overview of the Global Historical Climatology Network monthly mean temperature data set, version 3. *J. Geophys. Res.* **116**, D19121, DOI:10.1029/2011JD016187 (2011).
18. Wielicki, B. A. *et al.* Clouds and the Earth's radiant energy system (CERES): An Earth observing system experiment. *Bull. Am. Meteorol. Assoc.* **77**, 853–868 (1996).
19. Shindell, D. & Faluvegi, G. Climate response to regional radiative forcing during the twentieth century. *Nat. geosci.* **2**, 294–300 (2009).
20. Houze, R. A. *Cloud Dynamics*, pp 573, (Academic Press, San Diego, California, 1993).
21. Leibensperger, E. M. *et al.* Climatic effects of 1950–2050 changes in US anthropogenic aerosols – Part 2: Climate response. *Atmos. Chem. Phys.* **12**, 3349–3362 (2012).
22. Ramanathan, V. & Carmichael, G. Global and regional climate changes due to black carbon. *Nat. Geosci.* **1**, 191–197 (2008).
23. Zhang, Y., Wen, X. Y. & Jang, C. J. Simulating Climate-Chemistry-Aerosol-Cloud-Radiation Feedbacks in Continental U.S. using Online-Coupled WRF/Chem. *Atmos. Environ.* **44**, 3568–3582 (2010).
24. Lohmann, U. &, Feichter, J. Global indirect aerosol effects: a review. *Atmos. Chem. Phys.* **5**, 715–737 (2005).
25. Menon, S., Hansen, J. E., Nazarenko, L. & Luo, Y. Climate effects of black carbon aerosols in China and India. *Science* **297**, 1950–1953 (2002).
26. Yu, S. C. The role of organic acids (formic, acetic, pyruvic and oxalic) in the formation of cloud condensation nuclei (CCN): a review. *Atmos. Res.* **53**, 185–217 (2000).
27. Kaufman, Y. J., Koren, I., Remer, L. A., Rosenfeld, D. & Rudich, Y. The effect of smoke, dust, and pollution aerosol on shallow cloud development over the Atlantic Ocean. *Proc. Natl. Acad. Sci. USA* **102**, 11207–11212 (2005).
28. Charlson, R. J. *et al.* Climate Forcing by Anthropogenic Aerosols. *Science* **255**, 423–430 (1992).
29. Augustine, J. A. & Dutton, E. G. Variability of the surface radiation budget over the United States from 1996 through 2011 from high quality measurements. *J. Geophys. Res.* **118**, 43–53 (2013).
30. U.S. EPA. *Our nation's air: status and trends through 2010* (2012).
31. Eder, B. & Yu, S. C. A performance evaluation of the 2004 release of Models-3 CMAQ. *Atmos. Environ.* **40**, 4811–4824 (2006).
32. Goldstein, A. H., Koven, C. D., Heald, C. L. & Fung, I. Y. Biogenic carbon and anthropogenic pollutants combine to form a cooling haze over the southeastern United States. *Proc. Natl. Acad. Sci. U. S. A.* **106**, 8835, doi:10.1073/pnas.0904128106 (2009).
33. Yu, S. C., Bhave, P. V., Dennis, R. L. & Mathur, R. Seasonal and regional variations of primary and secondary organic aerosols over the continental United States: Observation-based estimates and Model evaluation. *Environ. Sci. Technol.* **41**, 4690–4697 (2007).
34. Taylor, K. E., Stouffer, R. J. & Meehl, G. A. An Overview of CMIP5 and the Experiment Design. *Bull. Am. Meterol. Soc.* **93**, 485–498(2012).

35. Dai, A., Karl, T. R., Sun, B. & Trenberth, K. E. Recent trends in cloudiness over the United States: A tale of monitoring inadequacies. *Bull. Am. Met. Soc.* **87**, 597–606 (2006).
36. Watanabe, S. *et al.* (2011) MIROC-ESM 2010: model description and basic results of CMIP5-20c3m experiments. *Geosci. Model Dev.* **4**, 845–872 (2011).
37. Watanabe, S. *et al.* Anthropogenic changes in the surface all-sky UV-B radiation through 1850–2005 simulated by an Earth system model. *Atmos. Chem. Phys.* **12**, 5249–5257 (2012).
38. Takemura, T. *et al.* Simulation of climate response to aerosol direct and indirect effects with aerosol transport-radiation model. *J. Geophys. Res.* **110**, doi:10.1029/2004JD005029 (2005).
39. Quaas, J. *et al.* Aerosol indirect effects – general circulation model intercomparison and evaluation with satellite data. *Atmos. Chem. Phys.* **9**, 8697–8717 (2009).
40. Kumar, S., Kinter, J., Dirmeyer, P. A., Pan, Z. & Adams, J. Multidecadal Climate Variability and the "Warming Hole" in North America: Results from CMIP5 Twentieth- and Twenty-First-Century Climate Simulations. *J Climate* **26**, 3511–3527 (2013).
41. Mickley, L. J., Leibensperger, E. M., Jacob, D. J. & Rind, D. Regional warming from aerosol removal over the United States: Results from a transient 2010–2050 climate simulation. *Atmos. Environ.* **46**, 545–553 (2012)

Acknowledgments

We thank Prof. Susan Solomon for insightful discussions that led to a substantial strengthening of the manuscript, Prof. Daniel Rosenfeld and Dr. Christian Hogrefe for helpful comments. We thank the CERES, GHCNM, MODIS and WCRP CMIP5 groups for producing the data used in this paper. The United States Environmental Protection Agency through its Office of Research and Development funded and managed the research described here. It has been subjected to Agency's administrative review and approved for publication. Analyses and visualizations used in this study were produced with the Giovanni online data system, developed and maintained by the NASA GES DISC. We also acknowledge the MODIS mission scientists and associated NASA personnel for the production of the data used in this research effort. The part of this work is supported by the "Zhejiang 1,000 Talent Plan" and Research Center for Air Pollution and Health in Zhejiang University.

Author contributions

S.Y., K.A. and R.M. initiated the project and designed the experiments, S.Y. wrote the main manuscript. S.Y., K.A., R.M., J.P., Y.Z., C.N., B.E., K.F. and T.N. contributed to the interpretation and to manuscript preparation.

Additional information

Supplementary information accompanies this paper at http://www.nature.com/scientificreports

Competing financial interests: The authors declare no competing financial interests.

How to cite this article: Yu, S. *et al.* Attribution of the United States "warming hole": Aerosol indirect effect and precipitable water vapor. *Sci. Rep.* **4**, 6929; DOI:10.1038/srep06929 (2014).